Activating mutations in *RRAS* underlie a phenotype within the RASopathy spectrum and contribute to leukaemogenesis

Elisabetta Flex[1,24], Mamta Jaiswal[2,24], Francesca Pantaleoni[1,25], Simone Martinelli[1,25], Marion Strullu[3,4,25], Eyad K. Fansa[2,25], Aurélie Caye[3,4], Alessandro De Luca[5], Francesca Lepri[6], Radovan Dvorsky[2], Luca Pannone[1], Stefano Paolacci[1], Si-Cai Zhang[2], Valentina Fodale[1], Gianfranco Bocchinfuso[7], Cesare Rossi[8], Emma M.M. Burkitt-Wright[9], Andrea Farrotti[7], Emilia Stellacci[1], Serena Cecchetti[10], Rosangela Ferese[5], Lisabianca Bottero[1], Silvana Castro[11], Odile Fenneteau[12], Benoît Brethon[13], Massimo Sanchez[10], Amy E. Roberts[14], Helger G. Yntema[15], Ineke van der Burgt[15], Paola Cianci[16], Marie-Louise Bondeson[17], Maria Cristina Digilio[6], Giuseppe Zampino[18], Bronwyn Kerr[9], Yoko Aoki[19], Mignon L. Loh[20], Antonio Palleschi[7], Elia Di Schiavi[11], Alessandra Carè[1], Angelo Selicorni[16], Bruno Dallapiccola[6], Ion C. Cirstea[2,21], Lorenzo Stella[7], Martin Zenker[22], Bruce D. Gelb[23], Hélène Cavé[3,4,26], Mohammad R. Ahmadian[2,26] & Marco Tartaglia[1,26]

[1]Dipartimento di Ematologia, Oncologia e Medicina Molecolare, Istituto Superiore di Sanità, Rome, Italy. [2]Institut für Biochemie und Molekularbiologie II, Medizinische Fakultät der Heinrich-Heine Universitat, Düsseldorf, Germany. [3]Genetics Department, Robert Debré Hospital, Paris, France. [4]INSERM UMR_S940, Institut Universitaire d'Hématologie (IUH), Université Paris-Diderot Sorbonne-Paris-Cité, Paris, France. [5]Laboratorio Mendel, Istituto di Ricovero e Cura a Carattere Scientifico-Casa Sollievo della Sofferenza, Rome, Italy. [6]Ospedale Pediatrico "Bambino Gesù", Rome, Italy. [7]Dipartimento di Scienze e Tecnologie Chimiche, Università "Tor Vergata", Rome, Italy. [8]UO Genetica Medica, Policlinico S.Orsola-Malpighi, Bologna, Italy. [9]Genetic Medicine, Academic Health Science Centre, Central Manchester University Hospitals NHS Foundation Trust, Manchester, UK. [10]Dipartimento di Biologia Cellulare e Neuroscienze, Istituto Superiore di Sanità, Rome, Italy. [11]Istituto di Genetica e Biofisica "A. Buzzati Traverso", Consiglio Nazionale delle Ricerche, Naples, Italy. [12]Biological Hematology Department, Robert Debré Hospital, Paris, France. [13]Pediatric Hematology Department, Robert Debré Hospital, Paris, France. [14]Department of Cardiology and Division of Genetics, and Department of Medicine, Boston Children's Hospital, Boston, MA. [15]Department of Human Genetics, Radboud University Medical Centre, and Nijmegen Centre for Molecular Life Sciences, Radboud University, Nijmegen, The Netherlands. [16]Genetica Clinica Pediatrica, Clinica Pediatrica Università Milano Bicocca, Fondazione MBBM, A.O. S. Gerardo, Monza, Italy. [17]Department of Immunology, Genetics and Pathology, Uppsala University, Uppsala, Sweden. [18]Istituto di Clinica Pediatrica, Università Cattolica del Sacro Cuore, Rome, Italy. [19]Department of Medical Genetics, Tohoku University School of Medicine, Sendai, Japan. [20]Department of Pediatrics, Benioff Children's Hospital, University of California School of Medicine, and the Helen Diller Family Comprehensive Cancer Center, San Francisco, CA. [21]Leibniz Institute for Age Research, Jena, Germany. [22]Institute of Human Genetics, University Hospital of Magdeburg, Otto-von-Guericke-University, Magdeburg, Germany. [23]Mindich Child Health and Development Institute and Departments of Pediatrics and Genetics and Genomic Sciences, Icahn School of Medicine at Mount Sinai, New York, NY. [24]These authors contributed equally to this project. [25]These authors contributed equally to this project. [26]These authors contributed equally as the senior investigators for this project.

SUPPLEMENTARY MATERIAL

Supplementary Table S1. Leading RASopathy gene candidates predicted by mammalian protein interaction/functional association network analysis.

Supplementary Table S2. Clinical features of the subjects heterozygous for germline *RRAS* mutations.

Supplementary Table S3. Haematological features associated with germline or somatically acquired *RRAS* mutations.

Supplementary Table S4. *In silico* prediction of the functional impact of *RRAS* disease-associated mutations.

Supplementary Table S5. Molecular dynamics (MD) analyses.

Supplementary Table S6. *C. elegans* phenotypes resulting from expression of wild-type RAS-1 or the disease-associated RAS-1^{G27dup} mutant.

Supplementary Figure S1. Mammalian protein interaction/functional association network analysis constructed by using proteins known to be mutated in RASopathies as seed proteins.

Supplementary Figure S2. Germline and somatic disease-associated *RRAS* mutations.

Supplementary Figure S3. May-Grünwald-Giemsa stained bone marrow smears from *RRAS* mutation-positive patients at diagnosis of myeloid malignancies.

Supplementary Figure S4. Partial amino acid sequence alignment of human RRAS, KRAS, NRAS and HRAS proteins, together with representative RRAS orthologs showing conservation of mutated residues.

Supplementary Figure S5. Abolished GAP-stimulated GTP hydrolysis of the RRAS^{G39dup} mutant.

Supplementary Table S1. Leading RASopathy gene candidates predicted by mammalian protein interaction/functional association network analysis.

Gene name	Links	Links in background	Links to seed	Links in subnetwork	z-score
KSR2	10	373330	3	1169	16.80292
KSR1	60	373330	7	1169	15.74081
RALGDS	37	373330	5	1169	14.37168
SPRY2	17	373330	3	1169	12.79210
RRAS	69	373330	6	1169	12.46291
FRS2	18	373330	3	1169	12.41847
PARK7	32	373330	4	1169	12.33921
RGL2	53	373330	5	1169	11.88482
PIK3CA	71	373330	5	1169	10.14864
SPRY1	27	373330	3	1169	10.04257
EPB42	14	373330	2	1169	9.35753
BRAP	14	373330	2	1169	9.35753
RGS12	31	373330	3	1169	9.33203
RALB	56	373330	4	1169	9.14782
PLAU	15	373330	2	1169	9.02576
RET	35	373330	3	1169	8.74470
SGSM3	61	373330	4	1169	8.72902
ARAF	65	373330	4	1169	8.42836
SPRY4	40	373330	3	1169	8.13561
ITSN1	42	373330	3	1169	7.92225
SHC2	74	373330	4	1169	7.84058
RASGRP3	43	373330	3	1169	7.82104
PIK3R5	76	373330	4	1169	7.72387
BCR	47	373330	3	1169	7.44813
FLT1	22	373330	2	1169	7.36913
FARP2	85	373330	4	1169	7.24881
RRAS2	53	373330	3	1169	6.96769
GRB10	25	373330	2	1169	6.87923
RASSF2	25	373330	2	1169	6.87923
VAV1	96	373330	4	1169	6.75796
PLCE1	26	373330	2	1169	6.73465
RAP1GDS1	58	373330	3	1169	6.62379
NEK10	28	373330	2	1169	6.46849
MET	64	373330	3	1169	6.26363
SYNGAP1	65	373330	3	1169	6.20831
RASSF1	31	373330	2	1169	6.11733

Supplementary Table S2. Clinical features of the subjects heterozygous for germline *RRAS* mutations.

Patient #	NS1166	9802
Nucleotide change	c.163G>A	c.116_118dup
Amino acid change	p.Val55Met	p.Gly39dup
Sporadic/familial	unknown	sporadic
Origin of mutation	-	*de novo*
Age at last evaluation (years)	51	16
Sex	female	female
Prenatal findings	NA	polyhydramnios
Feeding difficulties	NA	+
Growth failure	NA	+
Short stature (<3rd centile)	-[1]	+
Facial features	triangular face, downslanting palpebral fissures, low-set ears, thick lips	triangular face, downslanting palpebral fissures, ptosis[2], low-set ears, thick lips
Low posterior hairline	+	+
Congenital heart defect	-	pulmonic stenosis
Hypertrophic cardiomyopathy	-	-
Short/webbed neck	-	-
Broad chest	+	+
Pectus deformity	-	-
Coagulation defects	-	-
Postnatal lymphedema	-	-
Ophthalmological problems	-	-
Motor delay / muscular hypotonia	-	Delayed acquisition of walking (20 months)
Cognitive deficits	-[3]	-
Ectodermal anomalies	-	-
Lentigines	-	-
Nevi	-	-
café-au-lait spots	-	+
Malignancy	+[4]	+[5]
Other		Crowded teeth, pyloric stenosis, glomerulonephritis, arthritis

NA, not available.
[1]10th centile.
[2]Congenital, surgically treated.
[3]Borderline cognitive abilities.
[4]Unspecified bone tumour (left leg) diagnosed during childhood.
[5]AML suspected to be secondary to JMML, with onset at 13 years (Supplementary Table S3). The condition was not associated with any germline/somatic mutation affecting previously identified RASopathy genes. Several complications occurred during treatment (renal failure, pulmonar infection, vein-occlusive disease), without complete remission. Death occurred at age of 16 by recurrence of the disease after 2 years of palliative treatment.

Supplementary Table S3. Haematological features associated with germline or somatically acquired *RRAS* mutations. Mutations characterise a subset of myeloid neoplasms with classical features of JMML (*i.e.*, monocytosis, low blast counts, presence of circulating myeloid progenitors, and elevated basophil counts) combined with atypical features, including late onset and rapid progression to AML. The latter, along with monosomy 7, are reminiscent of AML with myelodysplasia-related changes.

Patient	**9802**	**7615**	**14385**
Diagnosis	AML[1]	JMML[2]	JMML[2]
Gender	F	F	F
Age at onset (years)	13	10	13
Splenomegaly	yes	yes	no
Peripheral blood cell counts ($x10^9$/L)			
Platelets	663	47	180
White blood cells	11	7.4	14
Monocytes	1.3	1.5	4.6
Basophils	0.2	0.18	0.77
Myeloid precursors in peripheral blood (%)	14	15	10
Circulating undifferentiated myeloid blasts (%)	8	3.5	10
Bone marrow smear cytomorphology			
Undifferentiated myeloid blasts (%)	38	12	18
Myelodysplasia	+	+	+
In vitro growth of myeloid progenitors	microclusters only	microclusters only	+
Haemoglobin (g/L)	86	104	120
Fetal Haemoglobin	NA	5%	-
RRAS mutation	c.116_118dup p.Gly39dup (germline)	c.116_118dup p.Gly39dup (somatic)	c.260A>T p.Gln87Leu (somatic)
Concomitant RAS pathway mutations	-	*NRAS*, c.82A>G p.Q61R (somatic)	*NRAS*, c.35G>A[3] p.G12D (somatic)
BCR-ABL transcript	-	-	-
Karyotype (blasts)	46,XX,t(3;6)(q26;q26)[24] /46,XX[4]	45,XX -7[20] /46,XX[1]	45,XX -7

NA, not available.
[1]Secondary to JMML.
[2]Rapidly progressed to AML.
[3]The clonal architecture was investigated by sequencing the somatic *RRAS* and *NRAS* mutations in 62 individual colonies obtained by *in vitro* culture of myeloid precursors (30 CFU-GM and 32 CFU-M). All colonies exhibited both mutations.

Supplementary Table S4. *In silico* prediction of the functional impact of *RRAS* disease-associated mutations.

Nucleotide substitution	Amino acid change	SIFT	Mutation Taster	PolyPhen-2
c.163G>A	p.Val55Met	deleterious (Score = 0)	disease causing (P = 0.999999)	probably damaging ($Score_{HumVar}$ = 0.962)
c.116_118dup	p.Gly39dup	*not analyzable*	*not analyzable*	*not analyzable*
c.260A>T	p.Gln87Leu	deleterious (Score = 0)	disease causing (P = 0.999999)	probably damaging ($Score_{HumVar}$ = 0.975)

Supplementary Table S5. Molecular dynamics (MD) analyses. Structural properties of the p.Val55Met RRAS mutant (V55M) assessed before and after the structural transition observed in the MD simulation. Comparison with corresponding parameters of wild-type RRAS (WT) documents that the mutation affects the H-bonding network stabilising the GDP-RRAS complex, increases the solvent accessibility of the mutated residue, and promotes formation of a stable cluster involving Met^{55}, Tyr^{58} and Ile^{50} (Fig. 2).

Properties	WT		V55M	
	0-50 ns	100-200 ns	0-50 ns	100-200 ns
Number of H-bonds with GDP[1]	1.3 ± 0.7	1.0 ± 0.7	1.4 ± 0.6	0.01 ± 0.08
% of SAS[2] for the side-chain of residue Val^{55}/Met^{55}	27 ± 11	28 ± 11	25 ± 12	36 ± 11
% of contacts[3] between residues Val^{55}/Met^{55} and Ile^{50}	0.0	0.0	0.0	10.9
% of contacts[3] between residues Val^{55}/Met^{55} and Tyr^{58}	79.10	84.53	95.90	84.71
% of contacts[3] between residues Tyr^{58} and Ile^{50}	0.04	0.02	0.03	49.19

SAS, solvent accessible surface.
[1]Average number of the H-bonds between residues Val^{55}/Met^{55}, and Ser^{56} and GDP.
[2]The solvent accessible surface of the side-chain for residue Val^{55} (wild-type) or Met^{55} (mutant) is normalised as percentage with respect to the maximum values of 117 $Å^2$ (valine) and 160 $Å^2$ (methionine).
[3]Percentage of the simulation time with the two residues at a minimum distance lower than 4 Å.

Supplementary Table S6. *C. elegans* phenotypes resulting from expression of wild-type RAS-1 or the disease-associated RAS-1^{G27dup} mutant.

Transgene (dose of injection)	*N*	Pvl (%)	Egl (%)	Bag (%)
none	175	1.1	0.6	0.6
empty vector $_{(30\ ng/\mu l)}$	106	1.9	0.9	0.9
ras-1^{WT} $_{(30\ ng/\mu l)}$	103	15.5	12.7	9.7
ras-1^{G27dup} $_{(30\ ng/\mu l)}$	103	29.1[1]	28.2[2]	17.5
ras-1^{WT} $_{(100\ ng/\mu l)}$	94	18.1	17.0	14.9
ras-1^{G27dup} $_{(100\ ng/\mu l)}$	89	42.7[3]	41.6[3]	32.6[4]

Injections were carried out on N2 worms (wild-type background).
Strains: *ras-1*^{WT} and *ras-1*^{G27dup} indicate *hsp-16.41::ras-1*^{WT} and *hsp-16.41::ras-1*^{G27dup}, respectively; *ras-1*^{G27dup} results from the three-nucleotide insertion, c.82_83insGCG, corresponding to the RASopathy causative c.116_118dup in *RRAS*.
The concentration at which the plasmid has been injected is reported in parenthesis.
Worms were grown at 20 °C and heat-shocked at early L3 stage. Isogenic worms that had lost the transgene were cloned separately and used as controls.
N indicates the number of animals scored.
Pvl is the percent of adult worms with a protruding vulva.
Egl is the percent of animals with an increased number of eggs retained in the uterus (N > 22).
Bag is the percent of bag-of-worms animals counted up to 6 days post-fertilisation.
[1-4]Statistical significance of comparisons with worms expressing *ras-1*^{WT} at the corresponding dose of injection ([1]$P < 0.05$; [2]$P < 0.005$; [3]$P < 0.0005$; [4]$P < 0.01$). *P* values were calculated using 2-Tail Fisher's Exact Test.

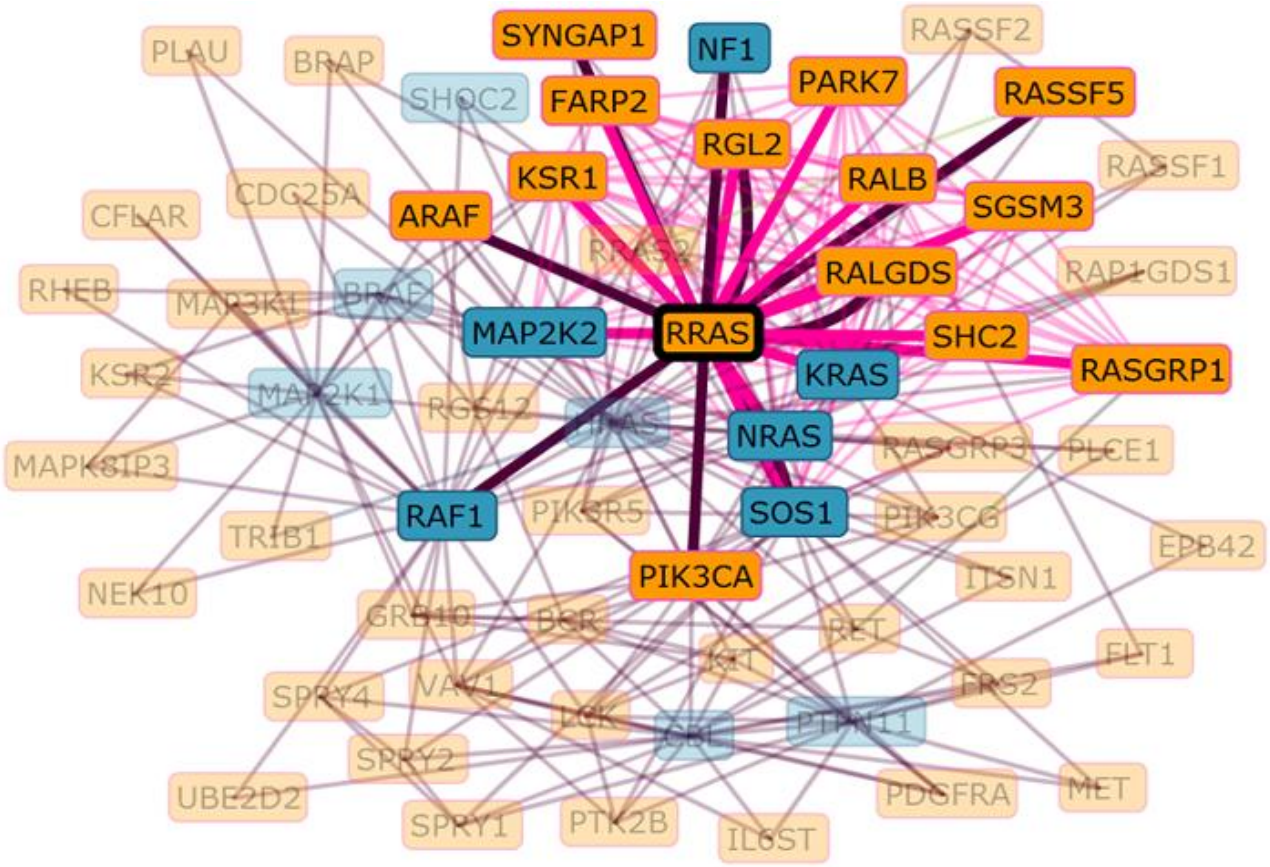

Supplementary Figure S1. Mammalian protein interaction/functional association network analysis constructed by using proteins known to be mutated in RASopathies as seed proteins. The analysis was performed by using Genes2FANs (15) (http://actin.pharm.mssm.edu/genes2FANs). Connections are based on Protein-Protein Interaction (PPI) and Connectivity Map (CMAP) networks, Mammalian Phenotype (MP) Browser, and Gene Ontology (GO), ChIP Enrichment Analysis (ChEA) and TRANSFAC databases. Connections involving RRAS are highlighted. Purple lines indicate protein-protein interactions; magenta lines indicate GO-biological process links. RASopathy genes are in blue. Leading candidates and relative z-scores are reported in Supplementary Table S1.

a

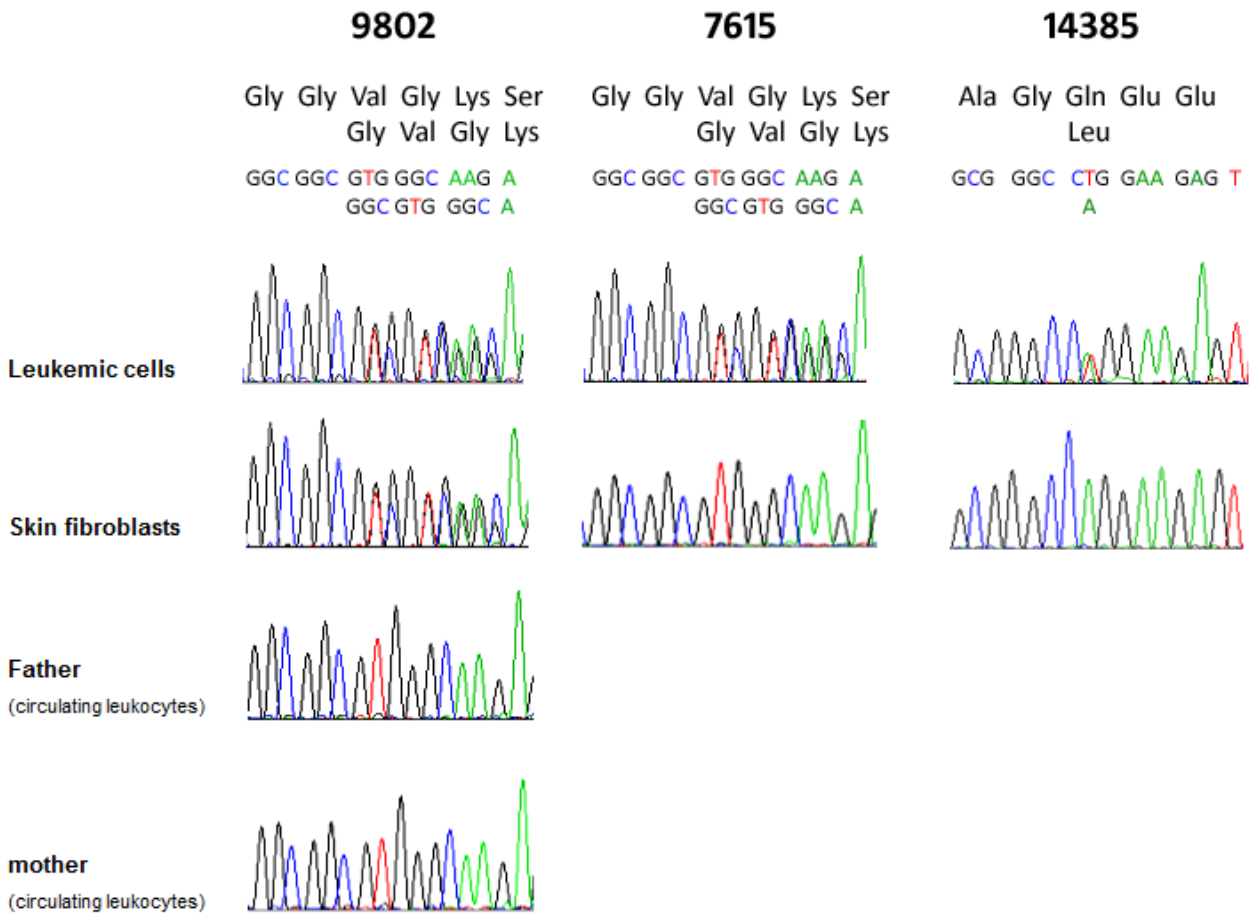

b

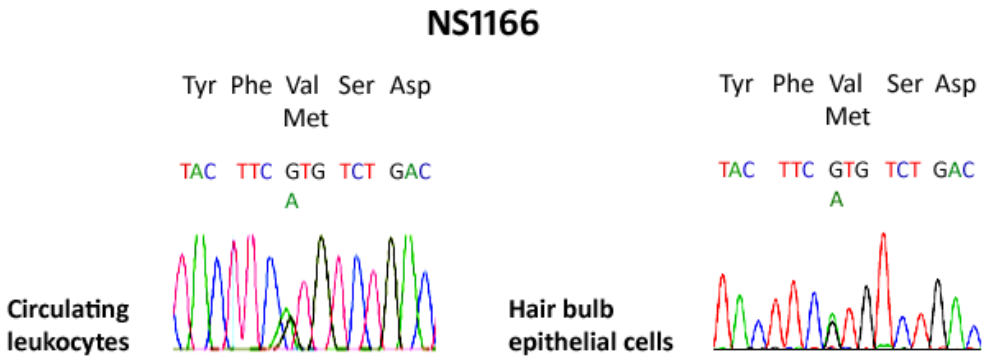

Supplementary Figure S2. Germline and somatic disease-associated *RRAS* mutations. (**a**) Electropherograms showing the *de novo*, germline origin of the c.116_118dup change (p.Gly39dup) in sporadic case 9802 (RASopathy with AML), and the somatic origin of the same in-frame duplication and the c.260A>T missense substitution (p.Gln87Leu) in subjects 7615 and 14385 (non-syndromic JMML). (**b**) Electropherograms of the germline c.163G>A missense substitution (p.Val55Met) in subject NS1166.

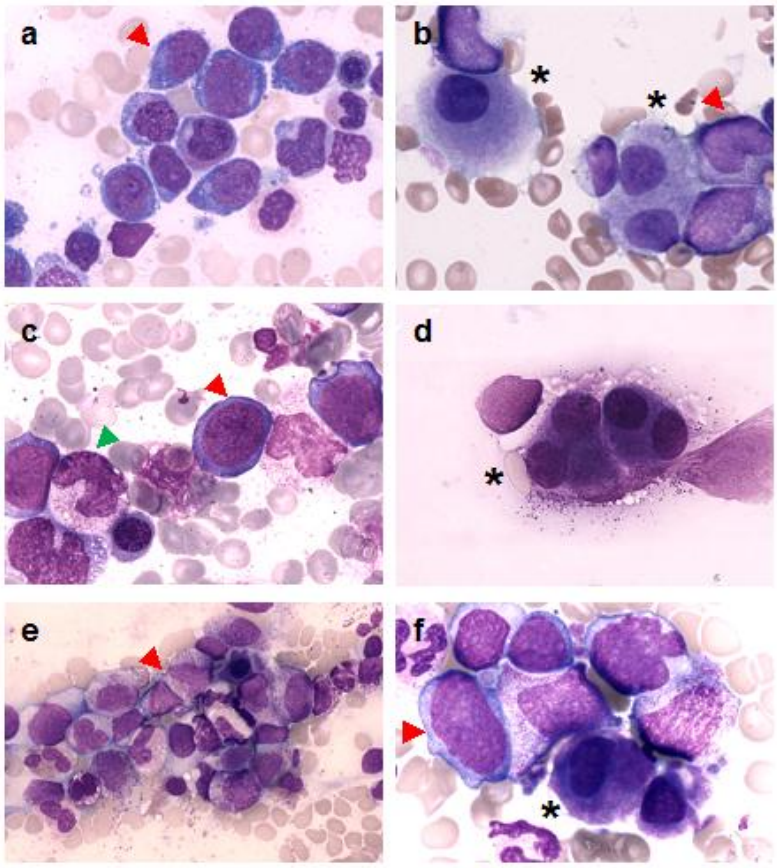

Supplementary Figure S3. May-Grünwald-Giemsa stained bone marrow smears from *RRAS* mutation-positive patients at diagnosis of myeloid malignancy. (**a**, **b**) Patient 9802 at the time of AML. (**c**, **d**) Patient 7615 with JMML. (**e**, **f**) patient 14385 with JMML. Morphological evidence of multilineage dysplasia together with excess of undifferentiated myeloid blasts is observed in all patients. Red arrowheads show undifferentiated myeloid blasts, while green arrowheads and black asterisks indicate dysplastic granulocytes and dysplastic micromegakaryocytes, respectively.

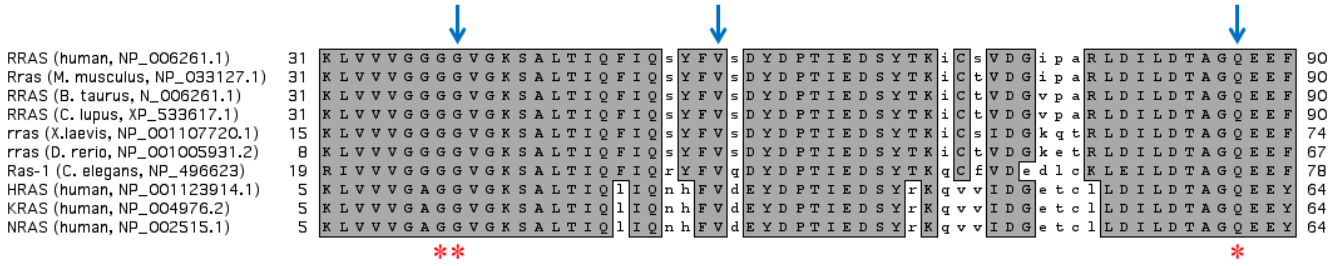

Supplementary Figure S4. Partial amino acid sequence alignment of human RRAS, KRAS, NRAS and HRAS proteins, together with representative RRAS orthologs showing conservation of the RRAS mutated residues. Blue arrows on top of the alignment mark amino acids affected by disease-associated *RRAS* mutations, while the red asterisks below the alignment indicate the positions of the cancer-associated mutation hot spots in RAS proteins.

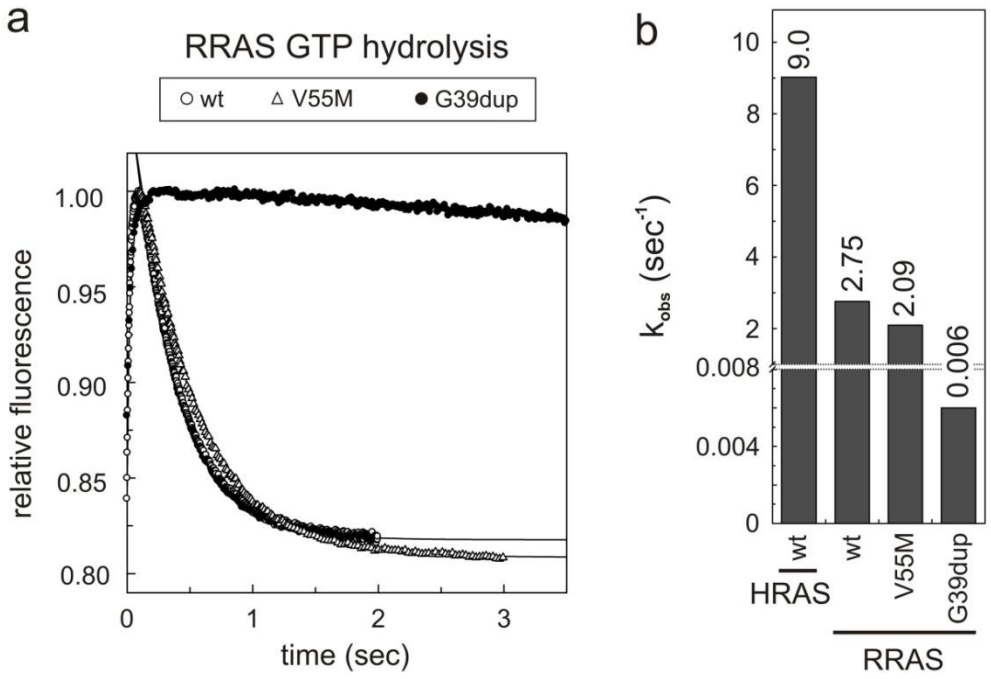

Supplementary Figure S5. Abolished GAP-stimulated GTP hydrolysis of $RRAS^{G39dup}$ mutant. (**a**) Kinetics of mantGTP hydrolysis of mantGTP-bound $RRAS^{WT}$, $RRAS^{V55M}$, and $RRAS^{G39dup}$ in presence of the GAP domain of neurofibromin. The decrease in fluorescence is directly correlated with the stimulated GTP hydrolysis reaction with an observed rate constant k_{obs} obtained by single exponential fitting and represented here as a bar chart (**b**). For comparison, the k_{obs} value for the GAP stimulated GTP hydrolysis of HRAS is shown.